Creating bandgaps in active piezoelectric slender beams through positive position feedback control

Kaczmarek, M.B.; Hassan HosseinNia , S.

DOI
10.1088/1361-665X/ad9443

Publication date
2024

Document Version
Final published version

Published in
Smart Materials and Structures

Citation (APA)
Kaczmarek, M. B., & Hassan HosseinNia , S. (2024). Creating bandgaps in active piezoelectric slender beams through positive position feedback control. *Smart Materials and Structures*, *33*(12), Article 125039. https://doi.org/10.1088/1361-665X/ad9443

Smart Materials and Structures

PAPER • OPEN ACCESS

Creating bandgaps in active piezoelectric slender beams through positive position feedback control

To cite this article: Marcin B Kaczmarek and S Hassan HosseinNia 2024 *Smart Mater. Struct.* **33** 125039

OPEN ACCESS
IOP Publishing
Smart Materials and Structures
Smart Mater. Struct. 33 (2024) 125039 (14pp)
https://doi.org/10.1088/1361-665X/ad9443

Creating bandgaps in active piezoelectric slender beams through positive position feedback control

Marcin B Kaczmarek* and **S Hassan HosseinNia**

Department of Precision and Microsystems Engineering, Delft University of Technology, Mekelweg 2, 2628 CD Delft, The Netherlands

E-mail: m.b.kaczmarek@tudelft.nl and s.h.hosseinniakani@tudelft.nl

Received 29 August 2024, revised 28 October 2024
Accepted for publication 17 November 2024
Published 28 November 2024

Abstract
Bandgaps—frequency ranges with reduced vibration transmissibility in elastic structures, are an opportunity for vibration control originating from the research on elastic metamaterials. In this paper, we study the design for bandgap in slender beams with collocated piezoelectric patch transducers. While creating bandgaps using shunted transducers is a well-established research field, using structures with piezoelectric sensors, actuators, and feedback controllers for the same application has not been thoroughly explored. This paper aims to study the use of the tools originating from the active vibration control (AVC) field for bandgap generation in finite beams with collocated piezoelectric sensors and actuators. Lightly damped second-order low-pass filters are used as controllers in the same configuration as positive position feedback, widely used for active damping. To facilitate the understanding of systems behaviour, we propose a simplified model based on the Euler–Bernoulli beam theory. A modal analysis approach and an assumption of an infinite number of transducers of infinitesimal length distributed along the structure are used to predict the frequency range of the locally resonant bandgap in closed form. The experimental part of the work demonstrates the feasibility of the proposed approach for creating bandgaps in practice. Thanks to the insights from AVC, the control system can be designed purely based on experimental frequency response data without the need for a parametric model of the system. We also show that the uniform distribution of actuators is not necessary for creating bandgap, which can be achieved in a structure with a relatively small number of sparsely placed actuators and compare the obtained results with analytical predictions for ideal metastructure. Low-frequency bandgaps placed between 10 and 320 Hz are obtained in experiments.

Keywords: metastructure, bandgap, active vibration control, positive position feedback, piezoelectric, feedback

* Author to whom any correspondence should be addressed.

1. Introduction

A bandgap,in the context of flexible structures, refers to a specific range of frequencies where the magnitude of the structures transmissibility is lower than 1. The idea originates from the research on elastic metamaterials but is promising for applications beyond this narrow field, for example, in vibration isolation of structures excited by narrow-band disturbances. Here, we focus on creating bandgaps in finite slender beams. For such structures, using piezoelectric patch transducers to obtain a bandgap is an appealing solution. Compact, highly integrated designs with such transducers can easily be created using existing, well-established technologies, and piezoelectric patch transducers can be easily retrofitted on existing components. Moreover, such a structure can have high stiffness, which is beneficial in many applications [1].

The methods for vibration control in piezoelectric smart structures can be divided into three categories, depending on the transducers' role, as illustrated in figure 1. While our focus is on feedback systems presented in 1(b), we also provide a description of the two remaining, with some representative examples from literature. Active and passive electronic elements and discrete controllers can be used in all the configurations. All the configurations can be used to implement tunable or adaptive systems. Moreover, in all cases, careless design and ignoring parasitic dynamics or time delays present in the system may result in instability.

In the approach presented in figure 1(a), piezoelectric transducers are shunted using electric or electronic circuits [2]. The majority of the results on bandgap creation in systems with piezoelectric transducers can be assigned to this category. Since the related literature is vast, we do not aim to provide an extensive review. Instead, we refer to a few selected papers with representative examples. All the transducers used in such a structure have the same role and are influenced in the same manner by the presence of the shunt (this is clearly seen when compared with feedback systems in figure 1(b), see e.g. the section on modeling in [3]). Single or connected transducers (like in figure 1(a)) can be used. The structure dynamics are altered due to the coupling with the shunt dynamics, which are often seen as a relationship between currents and voltages acting on the transducers. Active shunts can be implemented as 'voltage-controlled current-sources' [4–6], which offer greater design freedom and stronger influence on the structure's properties, for example, when 'negative capacitance' shunts are used [7–10].

In the structure presented in figure 1(b), transducers are divided into two groups: sensors and actuators, which operate under different conditions. Here, we only provide a brief description of the category and elaborate on the examples from the literature that fit it later in this section. The charge measured on the sensor is related to generalized displacement at its location. The external voltage applied to the actuator results in a generalized force applied to the structure [11]. The relationship between the signals of actuators and sensors can be seen as generalized stiffness. In the electronic circuits used to implement such a structure, subsystems for sensor signal conditioning, implementation of controller dynamics, and amplification of actuator signals can be identified. Both collocated and non-collocated sensors and actuators can be used.

In the approach presented in figure 1(c), the transducers are used in the self-sensing mode. The self-sensing refers to a single component acting as a sensor and actuator in a control system. While the term *self-sensing* is sometimes used to describe shunt circuits, like the one presented in figure 1(a) [12], there are other ways to implement this concept in vibration control with piezoelectric transducers. An overview of available methods can be found in [13]. All the transducers in the system have the same role, but the voltages applied to transducers are calculated based on the generalized displacements recovered by dedicated electronic circuits. For this reason, the same design approaches as for feedback systems presented in figure 1(b) can be used. To the best of our knowledge, this approach has not been used yet for the creation of bandgap in slender structures.

While the use of piezoelectric structures with shunts for bandgap creation is well-researched, the two other options have been neglected. The few results utilizing feedback are based on simple control methods, where the voltage of the sensor is proportional to the sensor voltage (related to generalized displacements) [14], its derivative with respect to time (related to generalized velocities), its second derivative with respect to time (related to generalized accelerations) [15, 16] or a linear combination of those terms [17] are used. In this way, the unit cells' effective stiffness, damping, or inertia are altered. Numerical analyses presented in these papers demonstrate widened bandgap regions, dependent on the controller gains when active feedback is used. While all aforementioned papers use collocated sensors and actuators, non-collocation is used to obtain non-reciprocal properties in [18].

In the scope of the classification presented in figure 1, the results utilising enhanced shunting circuits should also be categorised as feedback systems. The enhanced circuits presented in [3, 19, 20] consist of two collocated piezoelectric patch transducers. While the properties of one (the actuator) are influenced by the resonators present in the circuits, the other remains uninfluenced and acts as a sensor. In [19], the feedback loop consisting of a charge amplifier for sensor signal conditioning, a microprocessor for implementation of a digital controller and an actuator amplifier is studied. Feedback loops implemented in structures with collocated sensors and actuators using only analogue electronic elements have been used in [3, 20]. In all three papers, the influence of the feedback system on the structure was modelled by introducing frequency-dependent elastic moduli of the actuators, defined by the feedback loop dynamics. Dispersion properties of infinite metamaterial were analyzed using Bloch's boundary condition, and the behaviour of finite metastructures was shown experimentally.

Generating bandgaps in structures with sensors and actuators by actively implementing resonant dynamics in the feedback loop is a neglected research direction with great potential.

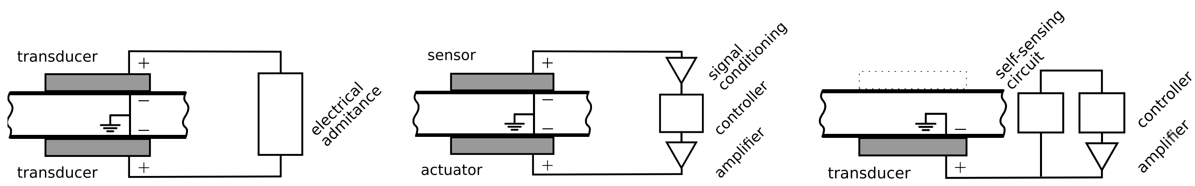

(a) Shunt (b) Feedback (c) Self-sensing feedback

Figure 1. Different configurations for vibration control in slender structures with piezoelectric transducers. In (a), all the transducers have the same role and the shunt is designed as an electrical impedance. In (b), transducers are divided into sensors and actuators, and the feedback controller can be seen as generalized stiffness. In configuration (c), only actuators are used in the system and the displacements at their locations, necessary to implement the feedback loop, are recovered using dedicated circuits.

The use of such smart structures for resonance peak damping, which is a closely related topic to bandgap creation, is well researched, and this knowledge can be translated to the bandgap problem (see examples in [11, 21]). While the feedback configuration is an alternative to commonly used shunt circuits, we do not claim it is better in any sense. We expect each configuration to have benefits and drawbacks depending on the application.

In this paper, we study bandgap generation in finite beams with collocated piezoelectric patch sensors and actuators, with the controller implemented digitally. To the best of our knowledge, the only paper studying such a configuration is [19]. What differentiates this work from [19] are the modeling and control approaches used. Lightly damped second-order low-pass filters are used as controllers, in the same configuration as in the positive position feedback (PPF) [11, 22] widely used for active damping. From the control theory perspective, bandgap generation in a finite structure is a rather simple problem, and the stability of the system can be easily assured using the negative imaginary (NI) systems theory if the underlying assumptions are satisfied [23]. For this reason, these aspects are not presented in the paper. The major advantage of the proposed control approach is that the practical design of the controller can be based on the experimental frequency domain data, without a need for a parametric model of the system. The paper's contributions focus on modelling the system, predicting the bandgap region in a finite structure and implementing the proposed approach practically.

To facilitate the understanding of systems behaviour, we propose a simplified model based on the Euler–Bernoulli beam theory, where the influence of each of the actuators is represented by a pair of moments related to the signal of the corresponding sensor. Bandgap analysis and predictions in [19] are based on the assumption of travelling waves in an infinite medium. However, this approach ignores the characteristics of finite structures and does not take advantage of the modal representation typically used for the analysis of such structures [24]. A method to predict a locally resonant bandgap in piezoelectric beams in shunt configuration under the assumption of an infinite number of transducers applied was developed in [25]. The approach was extended to piezoelectric metamaterial plates in shunt configuration in [26]. As a contribution of this work, we adopt the method developed in [25] to the piezoelectric metamaterial beams in sensor-actuator configuration and estimate the influence of a feedback loop on such a structure in a closed form under the same assumptions. The estimation is valid for arbitrary feedback loop dynamics that can be designed for active damping, bandgap generation or other objectives.

In the experimental part of the paper, we demonstrate that bandgap (seen as a significant reduction of vibration transmissibility magnitude below 1 at a selected frequency range) can be created in practice with the sensor and actuator configuration and feedback control. To the best of our knowledge, we are first to report such an achievement, as in [19], only resonance peak attenuation was presented experimentally using the studied configuration. We also show that the uniform distribution of actuators is not necessary for creating bandgap, which can be achieved in a structure with a relatively small number of sparsely placed actuators. We also acknowledge the importance of parasitic effects, not captured in the theoretical models and show their influence on the obtained bandgap by conducting numerical analysis in parallel to experiments.

The structure of the paper is as follows. Section 2 presents the model of the studied structures and the considered control system architecture. In section 3, we study the bandgap in metastructure using the assumption that an infinite number of transducers are placed on the structure. In section 4, we focus on smart structures with sparsely placed transducers and creating bandgaps in practice. Section 5 concludes the paper.

2. System description

The purpose of the model derived here is to provide insights into the behaviour of the system. The controllers used in the physical setup and presented in section 4 are tuned based on experimentally measured frequency response functions of the structure instead of analytical models. For this reason, a possibly simple model, not including the minute details of the system, is derived.

The system under consideration is schematically presented in figure 2. It consists of a beam with a rectangular cross-section embedded with S collocated piezoelectric sensor and actuator pairs. The objective of the control system is to limit the influence of base excitation and external disturbance forces on the vibrations of the structure at the point of interest at a targeted frequency range. The model of the structure, including the mechanical and electrical domains, which has been adopted from [25] by implementing the relationship between the

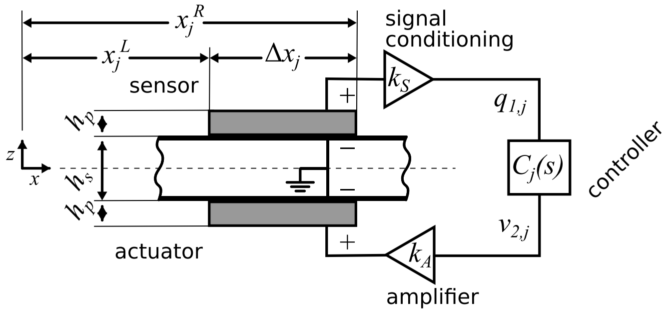

Figure 2. Schematic representation of the considered system. To simplify the modelling of the structure, the influence of the signal conditioning and actuator amplifiers are included in the model of the beam and represented by static gains. This approach is in line with the common practice in experimental system identification.

sensor signal, controller and voltage applied to the actuator, is presented in section 2.1. Section 2.2 presents the control-related aspects of the system.

2.1. Model of the system

We assume the beam has a constant cross-section consisting of two continuous and symmetrically located piezoelectric layers sandwiching a central substrate. The piezoelectric layers are poled in the thickness direction. The electrodes are segmented, forming transducer pairs on opposite sides of the beam, such that transducers in one layer have the role of sensors and, in the other, act as actuators. The electrode layers and bonding layers are treated as having negligible thickness. The slender composite beam, subject to specified boundary conditions, is modelled based on the Euler–Bernoulli beam theory, presuming geometrically small oscillations and linear-elastic material behaviour. For simplicity, it is assumed that the beam is undamped; however, the modal damping can be easily introduced later in the analysis.

In the model, the bending centre is assumed to be located at the geometric centre of the beams cross-section. However, due to the use of the sensor and actuator configuration of the piezoelectric transducers, the response of the bottom piezoelectric patch would be strongly distinguished from the upper one, which leads to a mismatch of the geometric centre and the bending centre locations and limited accuracy of the model. Nevertheless, the model sufficiently captures the system behaviour.

For the structure excited by some base displacement $w_b(t)$ and external transverse force with density $f(x,t)$ with relative vibration $w(x,t)$, the governing equations in physical coordinates are

$$\begin{aligned} &EI\frac{\partial^4 w}{\partial x^4}+m\frac{\partial^2 w}{\partial t^2} \\ &-k_A\vartheta\sum_{j=1}^{S}v_{2,j}(t)\frac{\mathrm{d}^2}{\mathrm{d}x^2}\left[H\left(x-x_j^L\right)-H\left(x-x_j^R\right)\right] \\ &=-m(x)\ddot{w}_b(t)+f(x,t), \end{aligned} \tag{1}$$

$$q_{1,j}(t)=k_S\vartheta\Delta w_j', \tag{2}$$

$$\ddot{y}(t)=\ddot{w}_b(t)+\ddot{w}(x_T,t), \tag{3}$$

where $w(x,t)$ is the transverse displacement of the beam at position x and time t, and $H(x)$ is the Heaviside function. $\ddot{y}(t)$ denotes the acceleration at the point of interest x_T. The segmented electrodes are numbered $j=1\ldots S$, with each electrode starting at $x=x_j^L$ and ending at $x=x_j^R$ with the total length $\Delta x_j=x_j^R-x_j^L$. The voltage $v_{2,j}(t)$ applied to the jth actuator is generated by an external amplifier with amplification factor k_A. The charge $q_{1,j}(t)$ measured at the jth sensor is proportional to the difference of slopes at the extremities of the transducer $\Delta w_j'=w'(x_j^R)-w'(x_j^L)$ [11], with a factor dependent of the signal conditioning circuit k_S. Furthermore, EI is the short circuit flexural rigidity, m is the mass per length, and ϑ is the electromechanical coupling term in physical coordinates, given by

$$EI=\frac{2b}{3}\left(c_\mathrm{s}\frac{h_\mathrm{s}^3}{8}+\bar{c}_{11}^E\left[\left(h_\mathrm{p}+\frac{h_\mathrm{s}}{2}\right)^3-\frac{h_\mathrm{s}^3}{8}\right]\right), \tag{4}$$

$$m=b\left(\rho_\mathrm{s}h_\mathrm{s}+2\rho_\mathrm{p}h_\mathrm{p}\right), \tag{5}$$

$$\vartheta=\bar{e}_{31}b\left(h_\mathrm{s}+h_\mathrm{p}\right), \tag{6}$$

c_s, ρ_s, and h_s are the central substrate layer's elastic modulus, mass density, and thickness, respectively, while b is the width of the beam. The piezoelectric layers have mass density ρ_p, thickness h_p, width b, elastic modulus at constant electric filed $\bar{c}_{11}^E$, effective piezoelectric stress constant $\bar{e}_{31}$, and permittivity component at constant strain $\bar{\varepsilon}_{33}^S$, where the overbars indicate effective material properties for 1D thin layers reduced from 3D constitutive equations as

$$\bar{c}_{11}^E=\frac{1}{s_{11}^E}, \tag{7}$$

$$\bar{e}_{31}=\frac{d_{31}}{s_{11}^E}, \tag{8}$$

where s_{11}^E is the elastic compliance at constant electric field, d_{31} is the piezoelectric strain constant.

Using an assumed-modes type expansion with N modes, the transverse displacement of the beam is expanded as

$$w(x,t)=\sum_{r=1}^{N}\phi_r(x)\eta_r(t), \tag{9}$$

where $\eta_r(t)$ are the modal weighting and $\phi_r(t)$ are the mode shapes of the beam for a given set of boundary conditions (at short circuit) normalized such that

$$\int_0^L m\phi_r(x)\phi_s(x)=\delta_{r,s},\quad r,s=1,2,\ldots \tag{10}$$

$$\int_0^L EI\phi_r(x)\frac{\mathrm{d}^4\phi_s}{\mathrm{d}x^4}\mathrm{d}x=\omega_r^2\delta_{rs},\quad r,s=1,2,\ldots \tag{11}$$

where L is the length of the beam, ω_r is the rth natural frequency, and δ_{rs} is the Kronecker delta. Note that (11) can be written in symmetric form

$$\int_0^L EI\frac{\mathrm{d}^2\phi_r}{\mathrm{d}x^2}\frac{\mathrm{d}^2\phi_s}{\mathrm{d}x^2}\mathrm{d}x = \omega_r^2\delta_{rs}, \quad r,s=1,2.$$

Substituting (9) into (1)–(3), multiplying by some mode shape $\phi_k(x)$, and integrating across the beam, the governing equations can be obtained in modal coordinates as

$$\ddot{\eta}_r(t)+\omega_r^2\eta_r(t)-k_A\vartheta\sum_{j=1}^{S}v_{2,j}(t)\,\Delta\phi'_{r,j}=q_{w,r}(t)+q_{f,r}(t), \tag{12}$$

$$q_{1,j}(t)=k_S\vartheta\sum_{r=1}^{N}\Delta\phi'_{r,j}\eta_r(t), \tag{13}$$

$$\ddot{y}(t)=\ddot{w}_b(t)+\sum_{r=1}^{N}\phi_r(x_T)\,\ddot{\eta}_r(t), \tag{14}$$

where the free indices r and j are assumed to go from $1\ldots N$ and $1\ldots S$, respectively,

$$\Delta\phi'_{r,j}=\left(\frac{\mathrm{d}\phi_r}{\mathrm{d}x}\right)_{x_j^L}^{x_j^R}=\frac{\mathrm{d}\phi_r}{\mathrm{d}x}\left(x_j^R\right)-\frac{\mathrm{d}\phi_r}{\mathrm{d}x}\left(x_j^L\right)$$

is the difference in slope of the r th mode between the ends of the j th electrode and the modal forcing is given by

$$q_{w,r}(t)=-\ddot{w}_b(t)\int_0^L m\phi_r(x)\,\mathrm{d}x, \tag{15}$$

$$q_{f,r}(t)=\int_0^L f(x,t)\,\phi_r(x)\,\mathrm{d}x. \tag{16}$$

Taking the Laplace transform of the governing equations we obtain

$$\left(s^2+\omega_r^2\right)H_r(s)-k_A\vartheta\sum_{j=1}^{S}V_{2,j}(s)\,\Delta\phi'_{r,j}=Q_{w,r}(s)+Q_{f,r}(s), \tag{17}$$

$$Q_{1,j}(s)=k_S\vartheta\sum_{r=1}^{N}\Delta\phi'_{r,j}H_r(s), \tag{18}$$

$$\ddot{y}(s)=\ddot{w}_b(s)+\sum_{r=1}^{N}\phi_r(x_T)\,s^2H_r(s), \tag{19}$$

where, with some abuse of the notation, $H_r(s), V_{2,j}(s), Q_{1,j}(s), Y(s), Q_{w,r}(s), Q_{f,r}(s)$ denote Laplace transforms of the time signals $\eta_r(t), v_{2,j}(t), q_{1,j}(t), y(t), q_{w,r}(t), q_{f,r}(t)$.

To study the transmissibility of the system, it is beneficial to express the base excitation in terms of acceleration. This leads to the modal forcing in the Laplace domain

$$Q_{w,r}(s)=-\ddot{w}_b(s)\int_0^L m\phi_r(x)\,\mathrm{d}x. \tag{20}$$

Focusing on the measurable signals we have then

$$\begin{aligned}Q_{1,j}(s)&=k_Sk_A\vartheta^2\sum_{k=1}^{S}\sum_{r=1}^{N}\frac{\Delta\phi'_{r,j}\Delta\phi'_{r,k}}{s^2+\omega_r^2}V_{2,k}(s)\\&\quad-k_S\vartheta\sum_{r=1}^{N}\frac{\Delta\phi'_{r,j}}{s^2+\omega_r^2}\int_0^L m\phi_r(x)\,\mathrm{d}x\,\ddot{w}_b(s),\end{aligned} \tag{21}$$

$$\begin{aligned}\ddot{y}(s)&=k_A\vartheta\sum_{k=1}^{S}\sum_{r=1}^{N}\frac{s^2\phi_r(x_T)\,\Delta\phi'_{r,k}}{s^2+\omega_r^2}V_{2,k}(s)+\ddot{w}_b(t)\\&\quad-\sum_{r=1}^{N}\frac{s^2\phi_r(x_T)}{s^2+\omega_r^2}\int_0^L m\phi_r(x)\,\mathrm{d}x\,\ddot{w}_b(s).\end{aligned} \tag{22}$$

Taking into account that

$$\sum_{r=1}^{N}\phi_r(x_T)\int_0^L m\phi_r(x)\,\mathrm{d}x=1 \tag{23}$$

we have

$$\begin{aligned}\frac{\ddot{y}(s)}{\ddot{w}_b(s)}&=1-\sum_{r=1}^{N}\frac{s^2\phi_r(x_T)}{s^2+\omega_r^2}\int_0^L m\phi_r(x)\,\mathrm{d}x\\&=\sum_{r=1}^{N}\phi_r(x_T)\int_0^L m\phi_r(x)\,\mathrm{d}x\frac{\omega_r^2}{s^2+\omega_r^2}.\end{aligned} \tag{24}$$

2.2. Control structure

The controller dynamics describe the relationship between the measured sensor outputs and actuation inputs. While various control architectures are available in the literature, we consider only a multi-single-input, single-output (SISO) structure, where the voltage applied to jth actuator $v_{2,j}(t)$ depends only on the charge measured at the corresponding jth sensor $q_{1,j}(t)$

$$V_{2,j}(s)=C_j(s)\,Q_{1,j}(s). \tag{25}$$

A positive feedback interconnection is used. When the piezoelectric sensor and actuator are collocated, the transfer function between the corresponding signals

$$G_{Q_j/V_j}(s)=\frac{Q_{1,j}(s)}{V_{2,j}(s)}=k_Sk_A\vartheta^2\sum_{r=1}^{N}\frac{\Delta\phi'_{r,j}\Delta\phi'_{r,j}}{s^2+\omega_r^2} \tag{26}$$

has the characteristic pattern of alternating poles and zeros, which can be used to guarantee the stability of the SISO control system. In a multiple-input, multiple-output case, the stability properties of flexible structures with collocated sensors and actuators are captured by the NI systems theory [23]. Transfer functions of finite flexible structures with collocated (generalized) force inputs and (generalized) position outputs, like the one of the system considered in this paper, are strictly NI [23].

A PPF [11, 22] controllers in the SISO form are used, described by

$$C(s)=\frac{k_\mathrm{c}}{s^2/\omega_\mathrm{c}^2+2s\zeta_\mathrm{c}/\omega_\mathrm{c}+1}, \tag{27}$$

where $\omega_c, \zeta_c, k_c > 0$. The transfer function of PPF is characterized by a resonance peak, and thanks to the roll-off at high frequencies, the controller can be implemented in practice, as this minimizes the risk of destabilizing the system in the presence of parasitic dynamics and time delays.

To simplify the design of the control system, controllers for all transducer pairs have the same strictly NI dynamics $C(s)$ with individually selected gains. We select the gain for each controller C_j to be equal to the inverse of the steady-state value of the transfer function between $Q_{1,j}$ and $V_{2,j}$

$$C_j(s) = g_j C(s), \quad g_j = G^{-1}_{Q_j,V_j}(0). \tag{28}$$

With this control structure, the stability of the closed-loop system can be concluded using the NI theory when $C(0) \leqslant 1$.

Any experimental system inevitably includes parasitic dynamics and time delays. It is, therefore, essential to ensure that the dynamics of the structure can be accurately captured by an NI model in the relevant frequency range. Additionally, evaluating the stability margins of the collocated pairs $G_{Q_j,V_j}(s)C_j(s)$ is a quick way to notice possible challenges for the systems stability.

3. Bandgap in active metastructures

In this section, we consider bandgap formation using the feedback approach in a metastructure, which is a finite structure consisting of repeated identical unit cells. In section 3.1, we provide an approximate analysis method under the assumption of the infinite number of transducers applied. section 3.2 shows the influence of the PPF controller on the bandgap generation. In section 3.3, we validate the developed method and show its applicability for structures with a finite number of transducers in a numerical analysis.

3.1. Ideal case with $S \to \infty$ and $\Delta x_j \to 0$

In this section, using the approach introduced in [25], we approximate the dynamics of the system as $S \to \infty$ and $\Delta x_j \to 0$. A closed-loop description of the considered control system can be obtained by substituting (28), (18) into (17)

$$\begin{aligned}\left(s^2+\omega_r^2\right)H_r(s) - k_S k_A \vartheta^2 \sum_{j=1}^{S}\sum_{k}^{N} \Delta\phi'_{k,j}\Delta\phi'_{r,j} C_j(s) H_k(s) \\ = Q_{w,r}(s) + Q_{f,r}(s).\end{aligned} \tag{29}$$

The system of equations described by (29) cannot be readily solved for a simple analytical expression for the modal weightings $H_r(s)$ due to the coupling from the presence of transducers.

For each transducer pair, the gain of the controller is related to the steady-state value of the transfer function between the charge and voltage in the pair, as described in (28). Using (2) in the physical coordinates, for infinitesimally long transducers we have

$$\begin{aligned}\lim_{\Delta x_j\to 0} q_{1,j} &= k_S\vartheta\Delta w'_j = k_S\vartheta\frac{\Delta w'_j}{\Delta x_j}\Delta x_j \\ &= k_S\vartheta\frac{\mathrm{d}^2 w}{\mathrm{d}x^2}(x_j)\Delta x_j.\end{aligned} \tag{30}$$

The influence of the voltage $v_{2,j}$ applied to the jth actuator can be represented by a pair of moments $M_j = -k_A\vartheta v_{2,j}$ acting at the actuator's extremities [11]. The relationship between the voltage $v_{2,j}$ applied to the jth transducer and the local curvature of the beam is then

$$\frac{\mathrm{d}^2 w}{\mathrm{d}x^2}(x_j) = \frac{-1}{EI}M = k_A\frac{\vartheta}{EI}v_{2,j}. \tag{31}$$

Combining the two formulas we get

$$\lim_{\Delta x_j\to 0} q_{1,j} = k_S k_A\frac{\vartheta^2}{EI}\Delta x_j v_{2,j}, \tag{32}$$

$$\lim_{\Delta x_j\to 0} G_{Q/V,j}(0) = k_S k_A\frac{\vartheta^2}{EI}\Delta x_j. \tag{33}$$

By combining (29) with (28) and (33) we have

$$\begin{aligned}&H_r(s)\left(s^2+\omega_r^2\right) \\ &- k_S k_A\vartheta^2\sum_{j}^{S}\sum_{k}^{N}\Delta\phi'_{k,j}\Delta\phi'_{r,j}\frac{EI}{k_S k_A\vartheta^2}\frac{1}{\Delta x_j}C(s)H_r(s) \\ &= Q_{w,r}(s) + Q_{f,r}(s),\end{aligned} \tag{34}$$

$$\begin{aligned}&H_r(s)\left(s^2+\omega_r^2\right) - C(s)\sum_{k}^{N}\sum_{j}^{S} EI\frac{\Delta\phi'_{k,j}}{\Delta x_j}\frac{\Delta\phi'_{r,j}}{\Delta x_j}\Delta x_j H_r(s) \\ &= Q_{w,r}(s) + Q_{f,r}(s).\end{aligned} \tag{35}$$

In the limit as $\Delta x_j \to 0$, $S \to \infty$

$$\begin{aligned}&\lim_{S\to\infty}\lim_{\Delta x_j\to 0}\sum_{j}^{S} EI\frac{\Delta\phi'_{k,j}}{\Delta x_j}\frac{\Delta\phi'_{r,j}}{\Delta x_j}\Delta x_j \\ &= \int_0^L EI\frac{\mathrm{d}^2\phi_k}{\mathrm{d}x^2}\frac{\mathrm{d}^2\phi_r}{\mathrm{d}x^2}\mathrm{d}x = \omega_r^2\delta_{kr}.\end{aligned} \tag{36}$$

Although this simplification is only exact in the limiting case, it can serve as a good approximation for a finite number of electrodes, as has been shown in [25] for piezoelectric structures with shunts. Equation (35) then becomes

$$H_r(s)\left(s^2+\omega_r^2\right) - C(s)\omega_r^2 H_r(s) = Q_{w,r}(s) + Q_{f,r}(s). \tag{37}$$

The transfer function

$$\frac{H_r(s)}{Q_{w,r}(s)} = \frac{H_r(s)}{Q_{f,r}(s)} = \frac{1}{s^2+\omega_r^2(1-C(s))} \tag{38}$$

can be used to predict the bandgap location for certain excitations, for example, see [25], where the vibrations of the beam are excited by one of the piezoelectric patch transducers. It can be interpreted as generalized compliance, where the presence of the piezoelectric transducers and control systems leads to a frequency-dependent dynamic modal stiffness $1 + C(s)$.

When the goal of the bandgap is to prevent the excitation of a system by base vibrations, the relationship between $\ddot{y}$ and $\ddot{w}_b$ has to be considered. Taking into account (19), (20) and (23) we get

$$\begin{aligned} T(s) &= \frac{\ddot{y}(s)}{\ddot{w}_b(s)} \\ &= 1 - \sum_r^N \frac{s^2}{s^2 + \omega_r^2 (1 - C(s))} \phi_r(x_L) \int_0^L m\phi_r(x)\,\mathrm{d}x \\ &= \sum_r^N \phi_r(x_L) \int_0^L m\phi_r(x)\,\mathrm{d}x \left(\frac{\omega_r^2 (1 - C(s))}{s^2 + \omega_r^2 (1 - C(s))} \right). \end{aligned} \tag{39}$$

The results presented in (38) and (39) represent the influence of controller dynamics on bandgap generation and are valid for arbitrary controllers designed as described in (28). Note, that the generalized compliance (38) can be rewritten as

$$\frac{H_r(s)}{Q_{f,r}(s)} = \frac{1}{s^2 + \omega_r^2} \frac{1}{1 - \frac{1}{s^2 + \omega_r^2} \omega_r^2 C(s)},$$

which is equivalent to a feedback interconnection of the dynamics of the structure in the absence of the controller and the term related to the controller $-\omega_r^2 C(s)$. Using this, suitable controllers for generating bandgap in considered systems can be found by using the loop-shaping approach demonstrated in [27]. The same relationships could be used to find optimal controllers for such an application.

3.2. Bandgap generation with PPF

This section shows the feasibility of creating a bandgap with a PPF controller using relations (38) and (39). For (27) we obtain

$$\frac{H_r(s)}{Q_{f,r}(s)} = \frac{s^2/\omega_c^2 + 2\zeta_c s/\omega_c + 1}{(s^2 + \omega_r^2)(s^2/\omega_c^2 + 2\zeta_c s/\omega_c + 1) - k_c \omega_r^2}, \tag{40}$$

which is characterized by an anti-resonance at frequency ω_c and leads to bandgap boundaries

$$\omega_c \sqrt{1 - k_c} < \omega < \omega_c. \tag{41}$$

As in the classical active-damping case, the use of PPF leads to softening of the structure which can be seen by taking the steady-state value of (40) $\omega_r^{-2}(1 - k_c)^{-1}$. When the PPF controller (27) is used directly in (39) we obtain (42) (see the next page)

$$\begin{aligned} T(s) &= \sum_r^N \phi_r(x_L) \int_0^L m\phi_r(x)\,\mathrm{d}x \\ &\times \left(\frac{\omega_r^2 (s^2/\omega_c^2 + 2\zeta_c s/\omega_c + 1 - k_c)}{(s^2 + \omega_r^2)(s^2/\omega_c^2 + 2\zeta_c s/\omega_c + 1) - k_c \omega_r^2} \right), \end{aligned} \tag{42}$$

which, in the absence of damping, is characterized by an anti-resonance at $\omega_c \sqrt{1 - k}$. The poles of the transfer functions remain within the limits described in (41), so the bandgap will appear at the same range of frequencies. The relationship (41) suggests that with the gain $k_c = 1$ it is possible to create a marginally stable structure with a bandgap region spanning from the static regime to arbitrarily high frequency ω_c. However, due to time delays and parasitic dynamics present in any physical control system, the useable values of k_c and ω_c are limited for stability reasons.

The antiresonance in the transmissibility of a metastructure with a PPF controller not overlapping with the corner frequency of the controller ω_c may be inconvenient in many applications. For this reason, we propose a modified description for the controller

$$C(s) = \frac{k_c}{s^2/\omega_c^2 + 2s\zeta_c/\omega_c + 1 + k_c}, \tag{43}$$

which results in

$$\frac{H_r(s)}{Q_{f,r}(s)} = \frac{s^2/\omega_c^2 + 2\zeta_c s/\omega_c + 1 + k_c}{(s^2 + \omega_r^2)(s^2/\omega_c^2 + 2\zeta_c s/\omega_c + 1) + k_c s^2}, \tag{44}$$

and the closed-loop transmissibility given in (45) (see the next page).

$$\begin{aligned} T(s) &= \sum_r^N \phi_r(x_L) \int_0^L m\phi_r(x)\,\mathrm{d}x \\ &\times \left(\frac{\omega_r^2 (s^2/\omega_c^2 + 2\zeta_c s/\omega_c + 1)}{((s^2 + \omega_r^2)(s^2/\omega_c^2 + 2\zeta_c s/\omega_c + 1) + k_c s^2)} \right). \end{aligned} \tag{45}$$

In this case, the bandgap boundaries are

$$\omega_c < \omega < \omega_c \sqrt{1 + k_c}, \tag{46}$$

and an antiresonance at frequency ω_c appears in the transmissibility transfer function. The control system with (43) should be stable for any $k_c > 0$ in the absence of parasitic dynamics and time delays.

3.3. Finite number of transducers and validation of the bandgap size

In this subsection, we show that the infinite-transducer approximation and the resulting bandgap region predictions are accurate, for a sufficient number of uniformly distributed transducer pairs. All the controllers corresponding to the transducer pairs are tuned with the same parameters, as described in section 2.2. Consider a uniform cantilever beam of length L with S evenly spaced transducer pairs, such that $x_j^L = (j-1)L/S, x_j^R = jL/S$. The numerical studies presented here focus on the beam excited by the base motion. The systems response and the resonance frequencies can be obtained using the description in the modal domain (17)-(19) and common dynamical system techniques. Sets of plots showing the resonant frequencies and the transmissibility from base excitation to the tip acceleration for the cantilever beam are shown in figures 3 and 4.

Figure 3 shows the influence of the gain k_c on the width of the bandgap. The subsequent plots were generated using

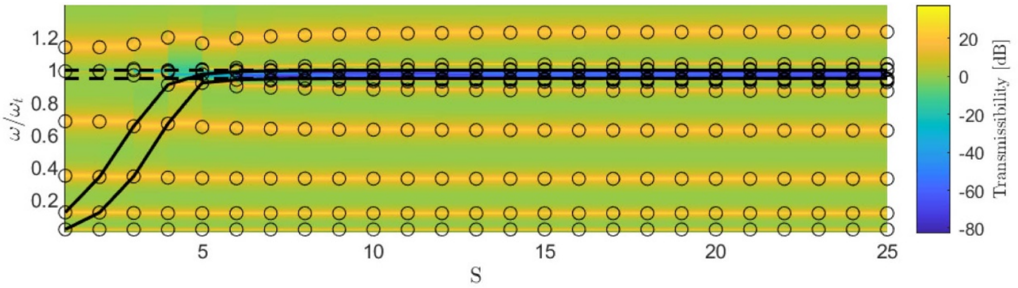

(a) $k_c = 0.1$

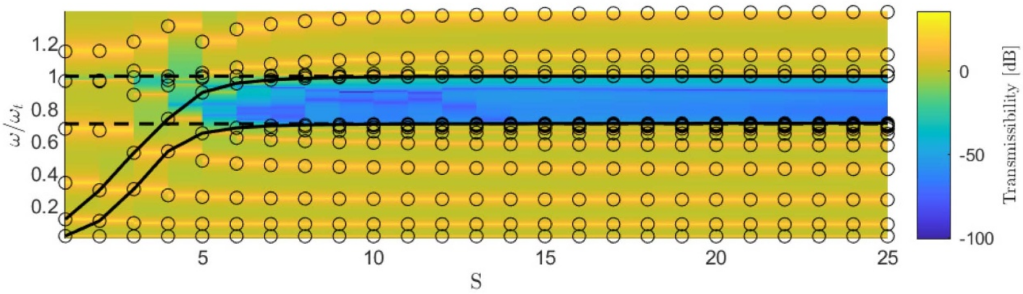

(b) $k_c = 0.5$

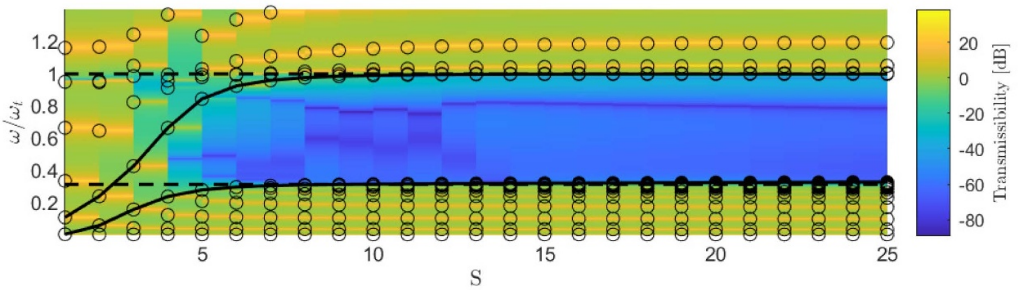

(c) $k_c = 0.9$

Figure 3. Transmissiblity and resonances of a finite length piezoelectric metastructure versus the number of unit cells S. Subfigures present the results for PPF controllers tuned target frequency $\omega_c = 50\omega_1$ with different controller gains k_c. Small circles indicate resonant frequencies of the full system, and the heatmap shows transmissibility on a log scale. Dashed lines show the expected bandgap edge frequencies for sufficiently large numbers of transducers. Solid lines track two resonances of the full system, ω_S and ω_{S+1}.

controllers with different values of k_c and the same remaining parameters. The bandgap region is indicated in the transmissibility plot by a reduction of magnitude over a range of frequencies. The solid lines in the plots highlight the resonant frequencies ω_S, ω_{S+1}, which according to [24] indicate the effective bandgap span. As S increases, the bandgap region converges to the theoretical prediction in (41). For increasing values of k_c the width of the badgap region increases in line with the prediction. What is interesting, for a structure with 4 transducer pairs, a wider region of transmissibility reduction can be seen, despite the presence of some resonance peaks within it.

Figure 4 shows the influence of the corner frequency ω_c on the behaviour of the system. The subsequent plots were generated using controllers with different values of ω_c and the same remaining parameters. The number of transducer pairs required for the limits of the bandgap region to converge to the theoretical prediction increases with the increasing ω_c. This may be related to the spatial resolution of the transducer array necessary for the shapes of the higher-frequency modeshapes.

In the studied cases of the active piezoelectric metastructure with a PPF controller, if the gain k_c is sufficiently high, the highest effective bandgap width achieved is the same as the theoretically predicted value (41). This is a different behaviour than in the case of metastructures with shunted piezoelectric transducers in [28] and metastructures with mechanical resonators in [24]. This may depend on the dynamics of the control element used and may require further investigation. Moreover, in some cases (for example figure 3(b) with $S = 4$) the transmissibility of the structure is lowered in a range of frequencies despite the presence of resonance peaks in the same range.

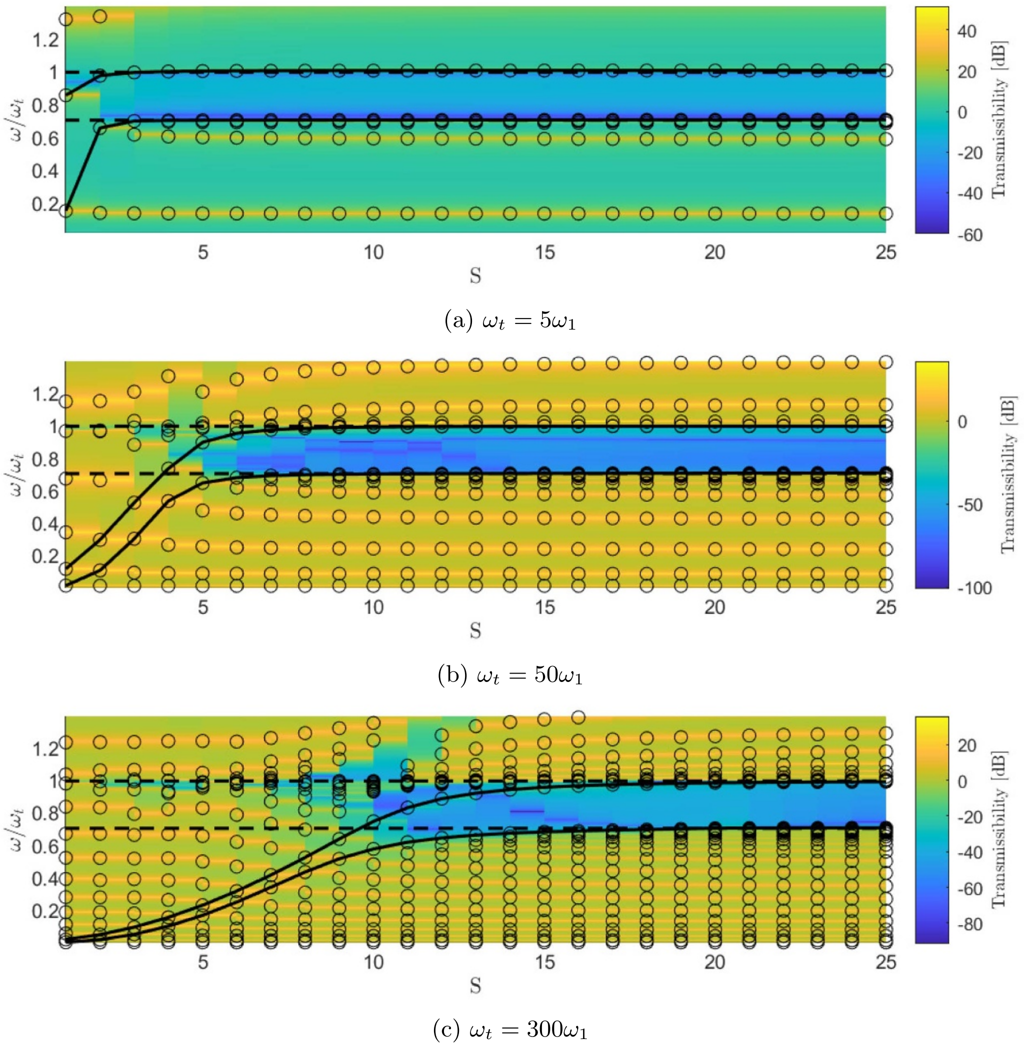

Figure 4. Transmissiblity and resonances of a finite length piezoelectric metastructure versus the number of unit cells S. Subfigures present the results for PPF controllers tuned with different target frequencies ω_c and the same controller gain $k_c = 0.5$. Small circles indicate resonant frequencies of the full system, and the heatmap shows transmissibility on a log scale. Dashed lines show the expected bandgap edge frequencies for sufficiently large numbers of transducers. Solid lines track two resonances of the full system, ω_S and ω_{S+1}.

4. Experimental structure with sparsely placed transducer pairs

This section demonstrates that the proposed feedback method can be used in practice for bandgap creation in structures with sensor and actuator configuration. The results presented here should not be seen as a validation of the approximation presented in section 3. Instead, we intend to compare the bandgap crated in realistic conditions and the bandgap edge frequencies expected in an ideal metastructure. Covering the entire structure with multiple small transducer pairs, which is required for the theoretical predictions to hold, may be impractical in many cases. The use of a high number of transducer pairs leads to a need for a high number of amplifiers for actuators and sensor signal conditioning. This drives the cost of a setup up and would discourage the use of bandgap in many practical applications.

The idea that periodicity is a requirement for wave attenuation and bandgap formation was demystified in [29], with an example of a finite beam with shunted piezoelectric transducers. Here, we show a similar result in a system in the feedback configuration.What is more, we show that, in some cases, such an arrangement may produce much wider bandgaps than the commonly used periodic arrangements. For transparency, we conduct the analysis in parallel on an experimental setup and its numerical model proposed in section 2. Despite the discrepancies, the model is sufficient to provide insights into system behaviour. The studied

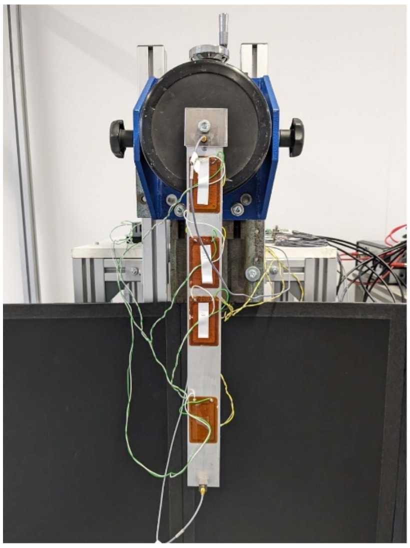

(a) Experimental setup

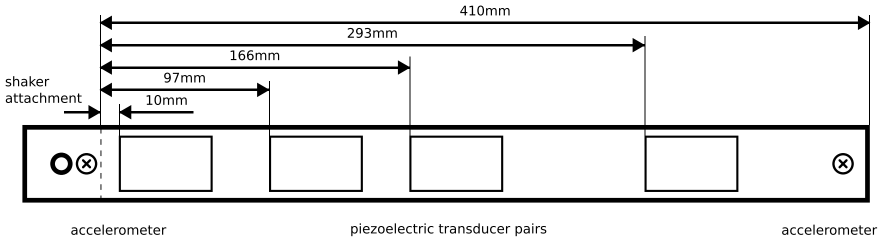

(b) Drawing of the experimental setup with dimensions

Figure 5. Illustration of the experimental setup. The main substrate of the structure is a slender aluminum alloy beam with thickness $h_s = 2$ mm and dimensions presented in 5(b). $\rho_s = 2700$ kg m^{-3} and $c_s = 69$ GPa assumed for simulations. Collocated piezoelectric patch transducers PI P-876.A15 DuraAct are used as both sensors and actuators.

experimental setup is presented in section 4.1. The open-loop characteristics are presented in section 4.2. The obtained bandgaps are shown in section 4.3.

4.1. Experimental setup

The studied structure is presented in figure 5, with the dimension of the setup in figure 5(b). The main substrate of the structure is a slender aluminum alloy beam, with $\rho_s = 2700$ kg m^{-3} and $c_s = 69$ GPa assumed for simulations. The base of the beam is clamped to vibration exciter Brüel & Kjaer type 4809 powred with amplifier Brüel & Kjaer type 2706. The vibrations of the tip and the base of the structure are measured by a pair of accelerometers Brüel & Kjaer 4508 B. Their signals are used to calculate the transmissibility of the system and determine the performance. Collocated piezoelectric patch transducers PI P-876.A15 DuraAct are used as both sensors and actuators. Four pairs of piezoelectric patch transducers are used to create bandgap in the structure. In-house-made charge amplifiers, based on TL074 operational amplifiers and designed as described in [30] with $C_f = 200$ nF and $R_f = 2$ MΩ are used to condition the signals of the sensors. The transfer function between the charge of the sensor and the amplifier voltage output is

$$\frac{V_0}{Q} = \frac{-R_f s}{(R_f C_f s + 1)\,(R_i\,(C_p + C_c)\,s + 1)}. \tag{47}$$

The two poles of the transfer function are $\omega_1 = 1/R_f C_f$ and $\omega_2 = 1/R_i(C_c + C_p)$ and the gain of the flat frequency band is $1/C_f$. Four Dual-Channel 300 V Amplifiers BD300 drive each of the actuators. The controllers are implemented digitally in the NI cRIO-9039 FPGA with the sampling frequency 10 kHz and the same system is used to monitor and record the performance signals. Module NI9215 is used to measure the sensor signals from charge amplifiers, module NI9234 is used for acceleration measurements and module NI9264 is used to generate excitation signals for the shaker and piezoelectric actuators.

The numerical model of the systems is created in the modal-domain based on (17)-(19) and common dynamical system techniques. The influence of the charge amplifiers for sensors and the high-voltage amplifiers for the actuators are modelled as static gains.

4.2. Open-loop results

The open-loop responses of the system (in the absence of control) have been measured by sending a frequency sweep signal to each of the input channels of the system separately. The open-loop frequency responses between the base and tip accelerations and signals of two pairs of sensors and actuators are compared with the model results in figure 6. Only 3 out of 5 input–output pairs are presented for clarity. The general characteristics of the system are well captured in the model. The differences in gain in the cross-coupling terms between the transmissibility and piezoelectric channels do not have a large influence on the accuracy of performance predictions, as will be demonstrated later. The diminishing magnitude of the experimental transmissibility, more clearly visible in figure 8, is caused by the influence of the mass of the accelerometer placed at the tip of the beam. Frequency responses between the voltage and charge of the collocated sensors and actuators are presented in figure 7. Here, the differences between the experimental setup and the model are clearly visible. While the

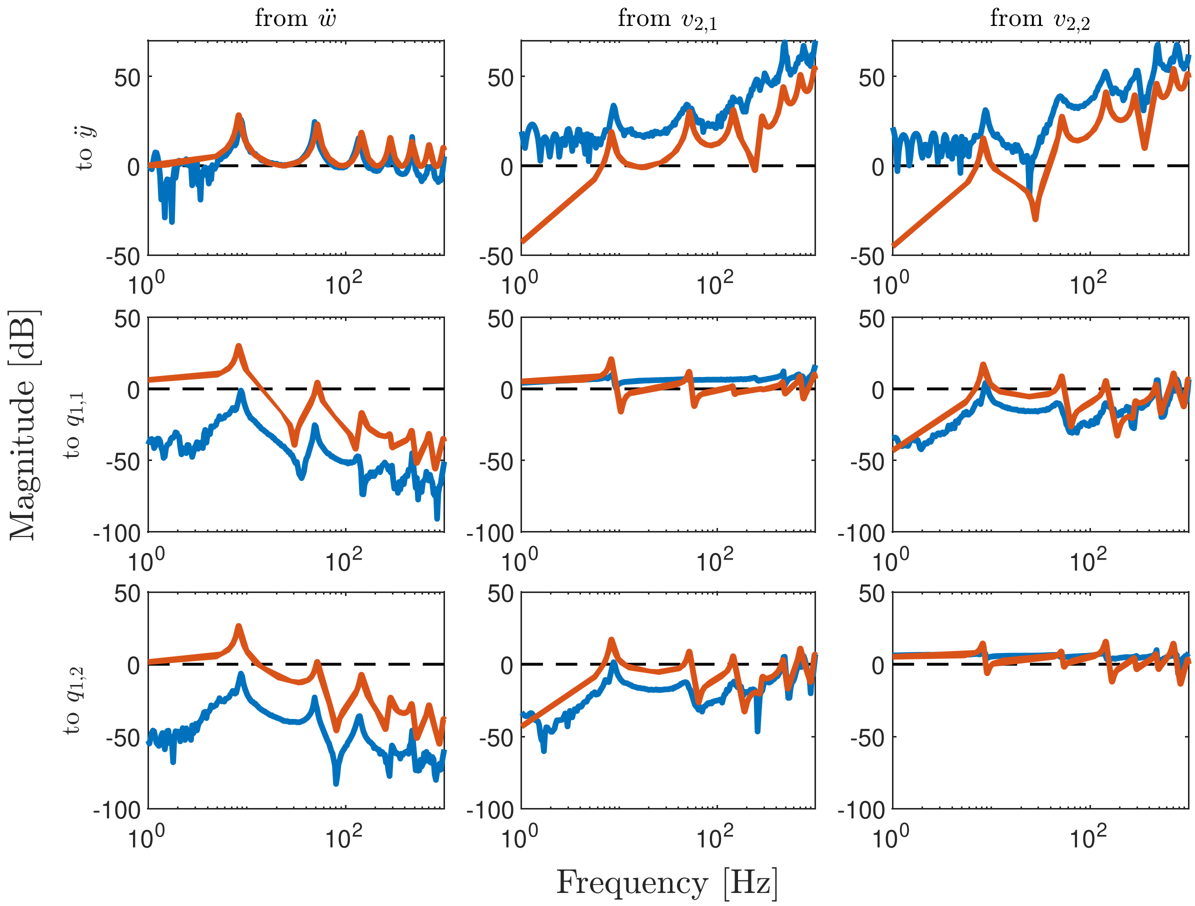

Figure 6. Open-loop magnitudes of the frequency response of the considered system, obtained from simulations (red) and experiments (blue). Only signals of two piezoelectric transducer pairs are presented for visibility.

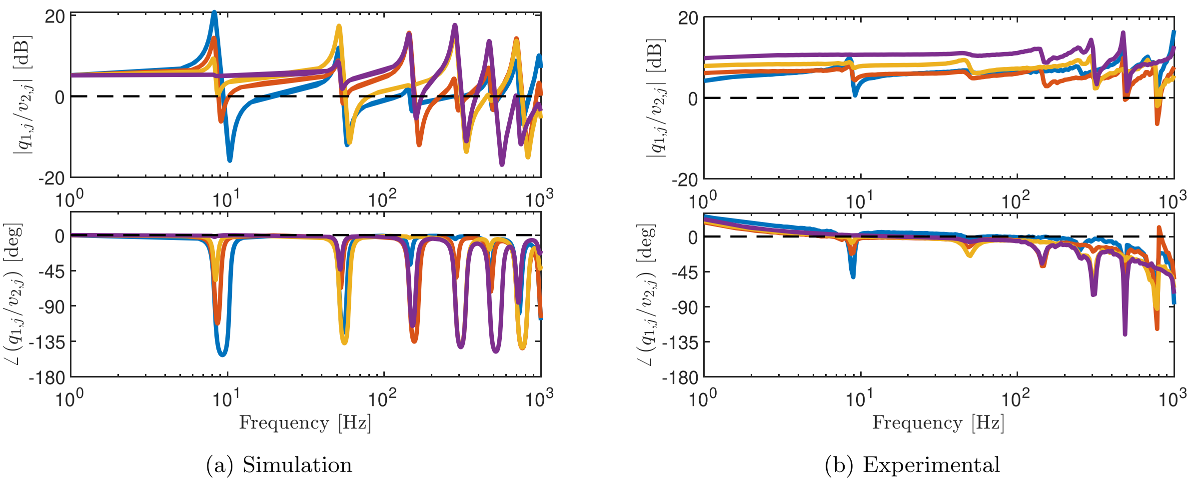

Figure 7. Frequency responses between the voltage and charge of the collocated sensors and actuators of the considered system. Each line corresponds to a different transducer pair.

model predicts that the low-frequency gains of the frequency responses should be the same, they differ in the experimental results. This could be caused by the manufacturing tolerances of the transducers, variations in the glueing of the transducers, soldering connections and alignment of the transducers. The influence of the charge amplifiers, not captured in the model, can be clearly seen in the experimental phase plot, where at low frequencies the phase exceeds the $0°$ asymptote. The influence of the time delay can be seen in the phase lag appearing at high frequencies. Despite these parasitic effects, in the studied frequency range between 5 Hz and 1000 Hz, the dynamics of the systems can be considered NI.

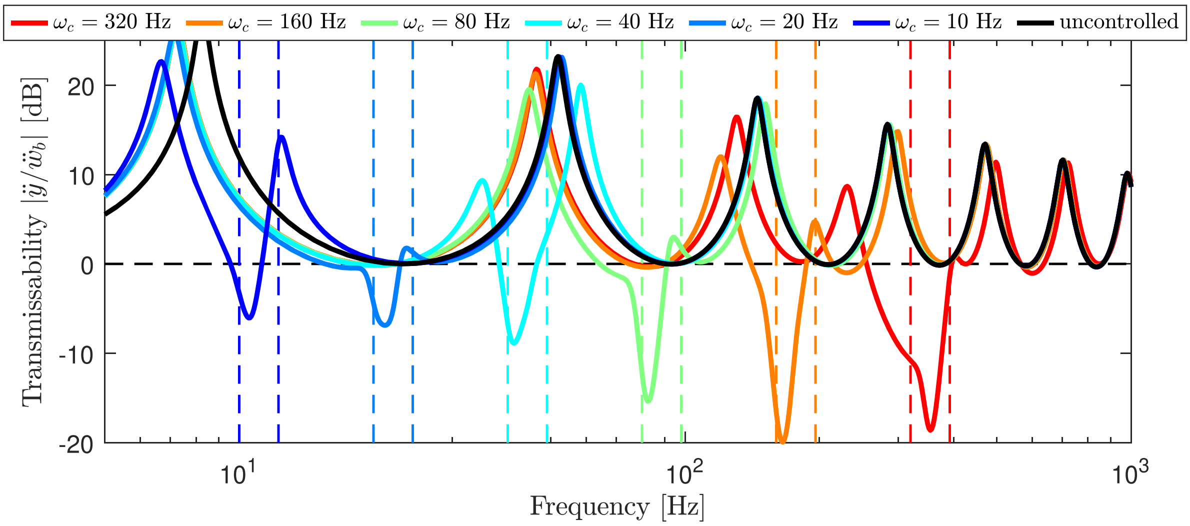

(a) Simulation

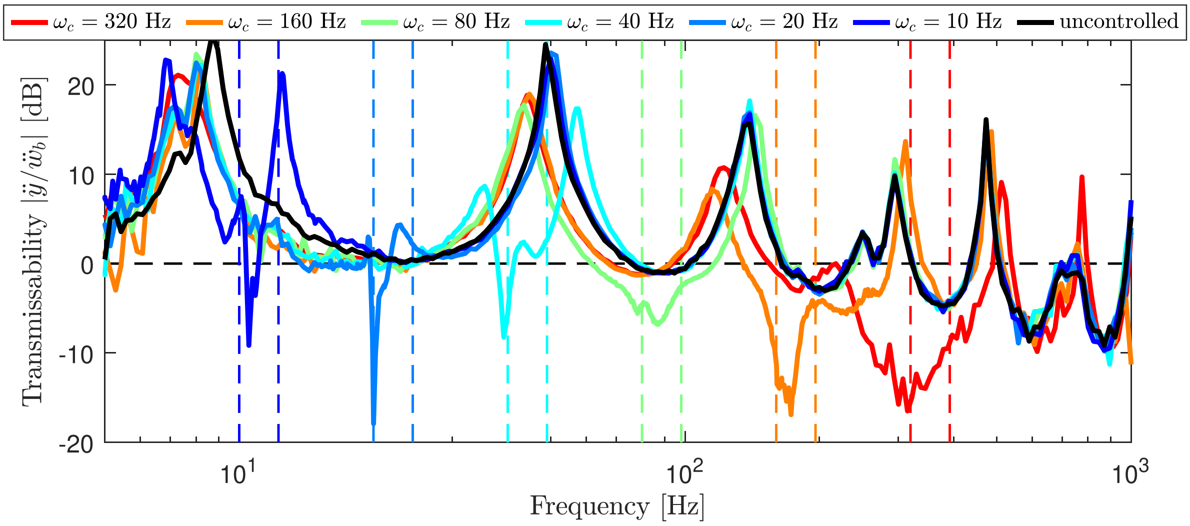

(b) Experiment

Figure 8. Transmissibility of the smart structures with sparsely placed transducers pairs, obtained from simulations and experiments. Different colour lines present the results with controllers tuned for different target frequencies and the same gain $k_c = 0.5$. Vertical dashed lines indicate the expected bandgap edge frequencies for a fully-covered metastructure with a sufficiently high number of transducer pairs.

4.3. Closed-loop results

In finite structures, the modal behaviour significantly influences the created bandgap. To showcase this, we consider bandgaps targeting different frequency ranges. Influencing the structure's behaviour is relatively easy close to resonance peaks since the high gain of the response of the structure leads to increased loop gain $|G_{Q_j/V_j}(s)C_j(s)|$. This case is well-researched in the active damping literature, where the objective of the controller is to reduce the magnitude of the resonance peaks of the structure. A bandgap targeting frequencies between resonance peaks may benefit structures excited by narrow-band disturbances. In such a case, the system's behaviour primarily depends on the controller's gain since the structure's response does not help with increasing the loop gain. While some related results in the active vibration control literature are available [31], this topic is significantly less studied than the active damping case. Exploring this, is a contribution of this work.

Figure 8 demonstrates the modelled and experimentally measured closed-loop bandgaps created using feedback control. The gains of the controllers were determined individually for each of the feedback loops according to (28), based on the corresponding modelled or measured transfer functions. The modified PPF controllers (43) were used to assure that the antiresonances in the transmissibility align with the target frequency ω_c. Bandgaps in different frequency ranges were created by assigning corresponding ω_c to all the controllers. The remaining tuning parameters were fixed at values $k_c = 0.5$ and $\zeta_c = 0.05$. These values were selected since they lead to stable closed-loop dynamics for a wide range of target bandgap frequencies, and possibly better results could be achieved by tuning them individually for each transducer pair and targeted frequency range. This however, is beyond the scope of this paper and should be the subject of future work. The transmissibilities with bandgaps at different frequencies have been plotted in different colours. Vertical lines in the same colours present the expected bandgap region boundaries, based on the infinite number of transducers assumption (46).

In all the considered cases, it was possible to create a bandgap region in the vicinity of the target frequency. The width of the bandgap strongly depends on the targetted range of frequencies. While bandgaps are narrower than boundaries expected in the ideal conditions in the lower frequency region, significantly wider bandgaps are obtained at higher frequencies. This effect may be related to the non-periodic arrangement of transducers on the structure and the large spacing between the transducers. Especially at higher frequencies, the obtained bandgap is related to the locations and the number of transducers. This effect is worth exploring to optimise the structure's design for bandgap generation.

Although the system's overall behaviour is well captured in the model, significant depth differences can be seen between the bandgaps obtained in the model and measured in the experiment. This highlights the importance of developing design methods based on the experimentally obtained, non-parametric models of the system, like frequency responses.

The differences in the lower frequency region (see bandgaps near 10 Hz and 20 Hz) can be attributed to the influence of the charge amplifier dynamics. The phase lead, clearly visible in figure 7(b) cancels the influence of the damping of the controller ζ_c at specific frequencies, leading to stronger attenuation. Using this effect for the benefit of the designer is also worth further studies. At higher frequencies (bandgaps near 80 Hz, 160 Hz, 320 Hz) the measured bandgaps are shallower than expected based on the model. We speculate that this is caused by the presence of noise in the system. If a deep bandgap is successfully implemented, the magnitude of the system response in the bandgap range is significantly reduced. This leads to a low signal-to-noise ratio. Moreover, in any closed-loop control system noise, originating for example from the electronics used in the system, is fed back to the actuators creating additional disturbance force.

The experimental results could be improved by reducing the noise levels in the system and using better-suited identification techniques. We expect that the noise can be eliminated to a large extent by improving the electronic implementation of the control system. Such improvements should include both low-noise power electronics for driving the actuators and more advanced circuits for sensor signal conditioning. To better identify the transmissibility of the system, attention should be paid to the selection of the excitation signal. The use of periodic signals gives access to a detailed nonparametric noise analysis and the identification could be further improved with local parametric methods (for example, see [32]).

5. Conclusions

Bandgaps—regions of reduced vibration transmissibility in elastic structures, are an opportunity for vibration control originating from the research on elastic metamaterials. In the case of slender structures, the use of piezoelectric patch transducers appears to be a well-suited solution. While the use of resonant shunts to create bandgaps is a well-researched topic, few results on obtaining bandgaps using feedback systems with piezoelectric sensors and actuators have been published so far.

We investigated this approach for creating bandgaps in finite beams. A simplified model of the system was developed and used for simulations. Using the assumption of an infinite number of transducers applied on the beam, we developed a method to estimate the influence of a feedback loop on a structure with piezoelectric sensors and actuators in closed form, which is valid for arbitrary feedback loop dynamics. The approximation's validity and the influence of a finite number of transducers on the bandgap generation were studied numerically. Additionally, we considered beams with a low number of sparsely placed transducer pairs and demonstrated that in such structures, bandgaps can be created using the proposed feedback approach, in some cases wider than in ideal metastructures.

The proposed approach for the design of feedback controllers for bandgap generation was validated experimentally, where clear bandgap regions at the target frequencies ranging between 10 and 320 Hz were measured. Possible improvements to these results can be achieved by modifying the electronic implementation of feedback systems to reduce noise levels and by applying more advanced identification techniques.

The presented approach can be extended to multiple PPF controllers in parallel to simultaneously create several bandgap regions. By correctly selecting the resonance frequencies and gains, merging the bandgap regions for attenuation in a wider frequency range should also be possible. The same stability condition, based on the NI systems theory, could be used.

Data availability statement

The data cannot be made publicly available upon publication because they are not available in a format that is sufficiently accessible or reusable by other researchers. The data that support the findings of this study are available upon reasonable request from the authors.

ORCID iDs

Marcin B Kaczmarek https://orcid.org/0000-0003-1469-2303
S Hassan HosseinNia https://orcid.org/0000-0002-7475-4628

References

[1] Soemers H 2010 *Design Principles for Precision Mechanisms* (University of Twente)
[2] Gripp J A B and Rade D A 2018 Vibration and noise control using shunted piezoelectric transducers: A review *Mech. Syst. Signal Process.* **112** 359–83
[3] Wang G and Chen S 2015 *Smart Mater. Struct.* **25** 015004

[4] Matten G, Collet M, Cogan S and Sadoulet-Reboul E 2014 *Proc. Technol.* **15** 84–89
[5] Nečásek J, Václavík J and Marton P 2016 Digital synthetic impedance for application in vibration damping *Rev. Sci. Instrum.* **87** 024704
[6] Yi K, Matten G, Ouisse M, Sadoulet-Reboul E, Collet M and Chevallier G 2020 *Smart Mater. Struct.* **29** 035005
[7] Bruneau H, Le Letty R, Claeyssen F, Barillot F, Lhermet N and Bouchilloux P 1999 Semipassive and semiactive vibration control using new amplified piezoelectric actuators *Smart Structures and Materials 1999: Smart Structures and Integrated Systems* vol 3668 pp 814–21
[8] Tang J and Wang K W 2001 *Smart Mater. Struct.* **10** 794–806
[9] Yu H, Wang K W and Zhang J 2006 *J. Sound Vib.* **295** 246–65
[10] Yi K and Collet M 2021 *J. Sound Vib.* **493** 115837
[11] Preumont A 2018 *Vibration Control of Active Structures* (*Solid Mechanics and Its Applications*) vol 246, 4th edn (Springer)
[12] Yi K, Liu Z and Zhu R 2022 *Smart Mater. Struct.* **31** 015042
[13] Jansen B, Butler H and Di Filippo R 2019 Active damping of dynamical structures using piezo self sensing *IFAC-PapersOnLine* **52** 543–8
[14] Yi K, Ouisse M, Sadoulet-Reboul E and Matten G 2019 *Smart Mater. Struct.* **28** 065025
[15] Li F, Zhang C and Liu C 2017 *J. Sound Vib.* **393** 14–29
[16] Ren T, Li F, Chen Y, Liu C and Zhang C 2020 *Compos. Struct.* **254** 112831
[17] Li Z Y, Ma T X, Wang Y Z, Chai Y Y, Zhang C and Li F M 2022 *Int. J. Solids Struct.* **254–255** 111865
[18] Banerjee A and Bera K K 2022 *Int. J. Mech. Sci.* **236** 107765
[19] Wang G, Cheng J, Chen J and He Y 2017 *Smart Mater. Struct.* **26** 025031
[20] Wang G, Wang J, Chen S and Wen J 2011 *Smart Mater. Struct.* **20** 125019
[21] Shivashankar P and Gopalakrishnan S 2020 Review on the use of piezoelectric materials for active vibration, noise, and flow control *Smart Mater. Struct.* **29** 053001
[22] Fanson J L and Caughey T K 1990 *AIAA J.* **28** 717–24
[23] Petersen I R and Lanzon A 2010 Feedback control of negative-imaginary systems: flexible structures with colocated actuators and sensors *IEEE Control Syst.* **30** 54–72
[24] Sugino C, Xia Y, Leadenham S, Ruzzene M and Erturk A 2017 *J. Sound Vib.* **406** 104–23
[25] Sugino C, Leadenham S, Ruzzene M and Erturk A 2017 *Smart Mater. Struct.* **26** 055029
[26] Sugino C, Ruzzene M and Erturk A 2020 An analytical framework for locally resonant piezoelectric metamaterial plates *Int. J. Solids Struct.* **182–183** 281–94
[27] Kaczmarek M B and HosseinNia H 2023 *Fractal Fract.* **7** 222
[28] Sugino C, Leadenham S, Ruzzene M and Erturk A 2016 *J. Appl. Phys.* **120** 134501
[29] Cardella D, Celli P and Gonella S 2016 *Smart Mater. Struct.* **25** 085017
[30] Karki J 2000 Signal Conditioning Piezoelectric Sensors - Application Report - Texas Instruments *Technical Report* (available at: www.ti.com/lit/an/sloa033a/sloa033a.pdf)
[31] Kim S-M, Brennan M J and Abreu G L C M 2016 *Mech. Syst. Signal Process.* **76–77** 47–57
[32] Schoukens J, Godfrey K and Schoukens M 2018 Nonparametric Data-Driven Modeling of Linear Systems: Estimating the Frequency Response and Impulse Response Function *IEEE Control Syst. Mag.* **38** 49–88